Hindawi
International Transactions on Electrical Energy Systems
Volume 2022, Article ID 1147096, 11 pages
https://doi.org/10.1155/2022/1147096

Research Article

Study on Steady-State Temperature Rise Characteristics of Motor Heat Balance under Load Rate

Feng Zhou,[1] **Pengfei Wang**,[1] **Xingzhen Bai**,[1] **Baochun Cui**,[1] **and Qiang Lyu**[2]

[1]*College of Electrical Engineering and Automation, Shandong University of Science and Technology, Qingdao, Shandong Province 266590, China*
[2]*State Grid of China Technology College, Jinan, Shandong Province 250002, China*

Correspondence should be addressed to Feng Zhou; f.zhou@163.com

Received 17 January 2022; Revised 5 May 2022; Accepted 11 May 2022; Published 29 June 2022

Academic Editor: B. Rajanarayan Prusty

The influence of load rate and other factors is not considered in the temperature rise monitoring process of traditional motor, which will lead to the wrong diagnosis of motor health status. In this paper, the characteristics of motor temperature rise under different ambient temperatures and different load factors are studied. Taking an 11 kW three-phase asynchronous motor as an example, the temperature rise model of the motor is based on the finite element method established using ANSYS software. The thermal conductivity coefficient and surface heat dissipation coefficient of each part of the motor are determined. According to the electromagnetic field calculation, the motor loss distribution is obtained, and the temperature rise distribution curve of the motor is obtained by the simulation of the three-dimensional steady temperature field of the motor. In this paper, the temperature rise variation law of the motor considering the influence of environmental temperature and load factors is proposed, and combined with the temperature rise threshold curve of the motor under different load rates, a dynamic threshold judgment system is established to accurately warn the motor of overheating under any load rate. When the motor's health status changes after running for a long time, it provides an important theoretical basis for accurate diagnosis of the motor's health status.

1. Introduction

The calculation of temperature and temperature rise of the motor is very important for the safe and stable operation of the motor. The temperature rise of the motor will change the physical, electrical, and mechanical properties of the windings. The excessively high motor temperature will directly cause insulation aging [1] and demagnetization of permanent magnet materials [2], which will affect the life and safe and reliable operation of permanent magnet motor. In severe cases, it will cause harm to the system and cause an abnormal shutdown of the motor.

Therefore, many experts and scholars at home and abroad have done professional research on the temperature rise of the motor. Luu et al. [3] established the electromagnetic model of permanent magnet synchronous motor (PMSM) and studied the interaction between temperature and electromagnetic field. Li et al. [4] from the Beijing Institute of Technology took a winding amorphous alloy stator tooth without magnetic yoke modular axial flux hub motor as an analysis prototype, established a three-dimensional temperature field finite element model of the motor, and obtained the amplitude and distribution of the temperature rise of the motor. Wu et al. [5], from Henan Polytechnic University, adopted the method of multifield coupling to study the distribution law of the transient temperature field of the motor under stable and unstable heat source conditions. Ma et al. [6] from Wuhan University of Technology used the finite element method to calculate the loss and temperature rise of the motor under three typical working conditions. Liu et al. calculated the thermal interaction boundary conditions of the motor by using Fourier's heat conduction law and Newton's law of heat release [7, 8]. Ge et al. [9] proposed a method to calculate gas friction loss based on the Bernoulli equation and obtained the temperature distribution law of the motor considering fluid velocity, temperature, and gas friction loss. Zhang et al. from Nanjing University of Aeronautics and Astronautics

used the finite element method to conduct thermal analysis on a double-salient pole brushless dc generator and proposed a thermal modeling method for flat wire [10, 11]. Zhang et al. [12] studied the temperature rise of the forced water-cooled motor and proved that the ambient temperature and cooling temperature would affect the temperature rise of the motor under the action of forced factors. In order to enhance the heat dissipation capacity of axial flux permanent magnet motor with high power density, Wu et al. [13] designed two new motor cooling structures: axial and internal circulating water cooling structure and internal and external circulating water cooling structure. Li et al. [4] took a winding amorphous alloy stator tooth no-yoke modular axial flux hub motor as an analysis prototype, established a three-dimensional electromagnetic field finite element model of the motor based on the electromagnetic loss theory of the motor, and calculated the amplitude and distribution of the temperature rise of the motor under different working conditions. Jiang et al. [14] proposed a design method to reduce the temperature rise of high-speed permanent magnet motor in vacuum environment. On the premise of guaranteeing both the starting torque and efficiency, iron consumption of the motor in steady-state operation was reduced.

The above literature plays an active role in the research of motor temperature and temperature rise. However, the above literature takes the standard ambient temperature and the temperature value and temperature rise of the motor in full load operation as the benchmark, without considering the influence of different ambient temperatures and load rates and other factors on the temperature rise of the motor. For example, for Class B insulation materials, the traditional thermal protection of small and medium-sized motors only uses the maximum allowable temperature of the motor windings (130°C) and the relative heat resistance index (>130~150) as the threshold for health diagnosis [15, 16] and did not consider the impact of ambient temperature and load rate on the health of the motor. This causes the monitoring system to make a false diagnosis of the motor's health.

In the actual operation of the motor, it is not always in full load state, and low load rate operation is common. However, the temperature and temperature rise threshold of the motor at full load are still the criteria to judge the motor's health status at low load rate. Therefore, when the motor thermal health problem occurs in the state of low load rate, the motor temperature rise does not reach the threshold, and the motor monitoring system cannot detect the fault, resulting in a small fault into a big fault affecting the safe and stable operation of the motor. In order to solve this problem, accurate thermal health diagnosis and early warning can be realized.

To sum up, this paper takes an 11 kW three-phase asynchronous motor as the research object. The temperature rise model of the motor based on the finite element method was established to determine the thermal conductivity coefficient and surface heat dissipation coefficient of each part of the motor. The distribution of iron loss, copper loss, and mechanical loss is calculated. The temperature rise distribution curve of the motor is obtained by simulating the three-dimensional steady temperature field of the motor. Considering the influence of ambient temperature and load factors, the research is carried out from the angle of temperature rise effect. The temperature rise variation law of motor under different working conditions is summarized, and the conversion law of temperature and temperature rise between stator, winding, and rotor is combined. A dynamic threshold judgment system which can accurately warn the motor overheating problem under arbitrary load rate is established. It provides an important theoretical basis for the design of motor temperature and temperature rise prediction system and also provides method support for thermal health diagnosis and early warning of intelligent motor system.

Table 1: Main parameters of the motor.

Structural parameter	Numerical
Rated power (kW)	11
Rated voltage (V)	380
Outer diameter of the stator (mm)	327
Rotor diameter (mm)	75
Stator slot number	72
Rotor slot number	58
Pole number	6
Rated speed (r/min)	978
Stray loss factor	0.02
Frequency (Hz)	50
Rated current (A)	6
Stator inner diameter (mm)	210
Maximum torque (N.m)	107.4
Stator slot type	2
Rotor slot type	2
Phase number	3
Air gap (mm)	0.35
Efficiency	85.53%

2. Determine Basic Motor Parameters

2.1. Motor Structure Parameter. This paper takes a model YZ200-6 forced air-cooled 11 kW three-phase asynchronous motor as the research object. The model is established in Maxwell according to the structural parameters of the motor. The structural parameters of the motor are shown in Table 1.

2.2. Material Properties. A variety of material properties such as resistivity, temperature rise coefficient, and specific heat capacity are required to build motor models in Maxwell. The main material properties are shown in Table 2.

2.3. Motor Model. To more conveniently calculate the temperature rise of the motor, this paper makes the following assumptions:

(1) The heat dissipation coefficient of the motor surface is constant, ignoring the thermal conductivity and the change of the heat dissipation coefficient with temperature

(2) Ignore the influence of the motor shaft

Table 2: Material properties of motor.

Motor parts	Material	Specific heat capacity (J/(kg·K))	Coefficient of thermal conductivity (W/(m·K))
Silicon steel core	M19_24G_2DSF0.920	450	42.5
Stator	M19_24G_2DSF0.920	450	42.5
Rotor	M19_24G_2DSF0.920	450	42.5
Rotor lamination	Cast_aluminum_75C	896	204
Stator winding	Copper	385	410
Inner region	Vacuum	1006.43	0.0242
Outer region	Vacuum	1006.43	0.0242
Shaft	Vacuum	1006.43	0.0242

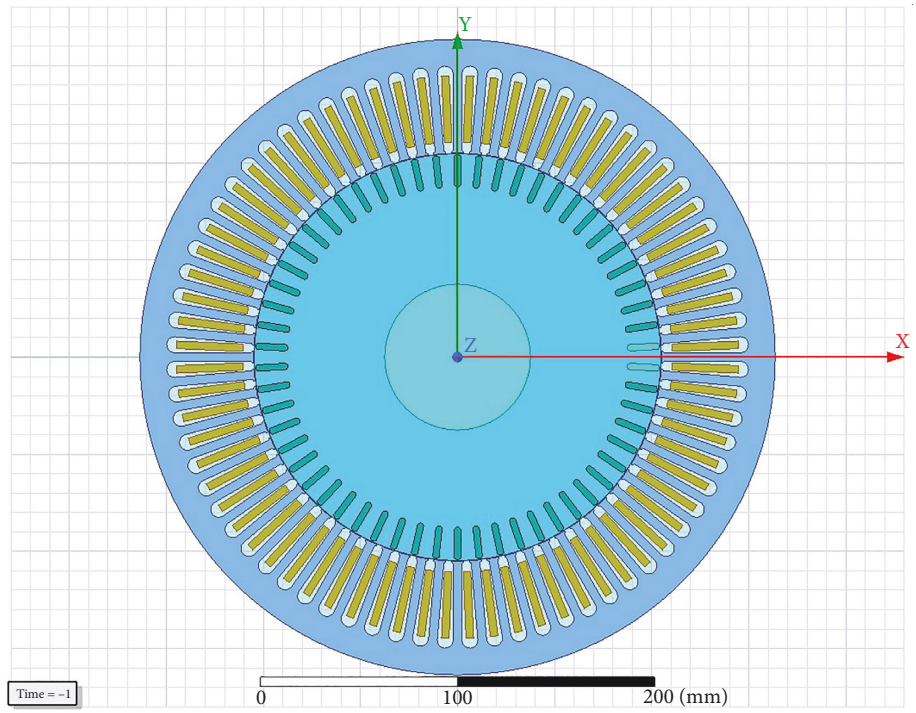

Figure 1: Geometric model of motor.

(3) All losses generated in the motor are converted into heat

(4) Motor iron consumption and rotor eddy current loss do not change with temperature

On the premise of meeting the above assumptions, the motor model is constructed in Maxwell using the above structural parameters and material properties, as shown in Figure 1.

3. Motor Loss Analysis Based on Bertotti Trinomial Method

When the ambient temperature changes a little, the temperature rise of the motor is mainly caused by the loss of the motor in the process of electromechanical energy conversion. Motor loss can be divided into four types: copper loss, iron loss, mechanical loss, and stray loss.

3.1. Copper Loss P_{Cu}. The copper loss of asynchronous motor consists of stator winding loss and rotor winding loss. Its size depends on the current in the winding, so the copper loss can be reduced by reducing the stator current and rotor current. The expression of copper loss is

$$P_{\mathrm{Cu}} = 3I^2R. \tag{1}$$

In (1), P_{Cu} is copper loss; I is the effective value of the stator phase current; R is the stator phase resistance.

3.2. Iron Loss P_{Fe}. At present, the iron loss calculation model proposed by Bertotti in 1988 is the most widely used and accurate method for stator iron loss calculation. Based on the loss mechanism, the Bertotti trinomial method divides the core loss into three parts: hysteresis loss [17], eddy current loss [18], and miscellaneous loss [19], and puts forward the loss calculation formula of each part to realize the loss separation. For each factor that affects the calculation accuracy of loss, the corresponding loss part can be found to be correct, which greatly improves the application scope and calculation accuracy of the model.

The iron loss of induction motor is mainly composed of hysteresis loss P_h and eddy current loss P_e. During the operation of the motor, the magnetic field in the silicon steel plate of the motor changes with the change of the current and the rotation of the rotor magnetic potential, and the changing magnetic field will produce hysteresis and eddy current loss. Hysteresis loss is the energy loss caused by the changing orientation of magnetic domains and the displacement of domain walls in iron cores under the action of alternating magnetic fields. Under the action of the alternating magnetic field, the induced current of the conductor forms power loss, which is called eddy current loss.

$$P_h = k_h(1+s)\omega_e\Phi_m^2 = k_h f B^\alpha, \tag{2}$$

$$P_e = k_e\left(1+s^2\right)\omega_e\Phi_m^2 = k_e(fB)^2, \tag{3}$$

$$P_{\mathrm{Fe}} = P_h + P_e = k_h f B^\alpha + k_e(fB)^2. \tag{4}$$

In (2)–(4), P_{Fe} is iron loss and P_h is hysteria loss. P_e is eddy current loss. K_h is the hysteresis loss coefficient; K_e is the eddy current loss coefficient; ω_e is the angular frequency of power supply; Φ_m is the air gap flux; S is the slip frequency. F is the magnetic field alternating frequency; B is the flux density, which changes sinusoidally; α is the empirical coefficient, usually $\alpha = 2$.

3.3. Mechanical Loss P_{mech}. Mechanical losses are generated during the operation of the motor and are mainly composed of fan friction losses and bearing friction losses. These losses are difficult to calculate under normal circumstances and are usually estimated based on empirical data and existing motor test data.

3.4. Stray Loss P_Δ. Stray loss refers to the sum of friction and wind resistance, stator and rotor copper loss, and no-load core loss not included in the total loss of the motor. These losses are difficult to calculate under normal circumstances and are usually estimated based on empirical data and existing motor test data.

The calculation results of parameter loss are shown in Table 3.

Table 3: Calculation results of loss.

Loss	Calculation results (W)
Stator winding copper loss	735.292
Rotor winding copper loss	251.921
Core loss	490.621
Mechanical loss	162.988
Stray loss	220
Total loss	1860.822

4. Calculation of Motor Heat Dissipation Coefficient considering Heat Balance

Heat transfer is a universal phenomenon in nature. As long as there is a temperature difference between objects or within objects, heat transfer phenomenon will occur. Heat transfer has three basic modes: heat conduction, heat convection, and heat radiation [20, 21]. In the medium and small induction motor thermal radiation produced by the heat dissipation is small. In this paper, the influence of heat radiation on the temperature rise of the motor is ignored, and only two modes of heat conduction and heat convection are considered.

4.1. Heat Conduction. Heat conduction usually occurs between bodies in contact. Since there is no relative displacement between bodies, heat depends on the thermal motion transmitted by microscopic particles. The thermal conductivity φ is usually calculated by the Fourier law of thermal conductivity.

$$\phi = -\lambda\frac{\mathrm{d}t}{\mathrm{d}x}. \tag{5}$$

In (5), λ is the thermal conductivity coefficient. $\mathrm{d}t/\mathrm{d}x$ is the rate of change of temperature.

4.2. Heat Convection. Heat transfer between a fluid and a solid that occurs in a motor is called convective heat transfer. The basic calculation formula is Newton's cooling formula.

$$\phi = hA\Delta t. \tag{6}$$

In (6), A is the convective surface. h is the convective heat transfer coefficient. Δt is the temperature difference between the two convection surfaces.

4.3. Calculation of Heat Dissipation Coefficient

4.3.1. Calculation of Heat Dissipation Coefficient of Motor. For the enclosed motor, the enclosure is the main way of external heat dissipation of the motor. The heat dissipation coefficient of the motor is closely related to the flow rate of the medium, the structure of the heat dissipation surface, and other cooling and heat dissipation conditions, which can be calculated according to the following formula:

$$\alpha = 14\left(1 + 0.5\sqrt{\omega_i}\sqrt[3]{\frac{\theta}{23}}\right). \tag{7}$$

In (7), α is the surface heat dissipation coefficient of the motor. ω_i is the wind speed of the inner wall of the frame. θ is the temperature of the outer surface of the frame wall.

Due to the difference between the 2d simulation calculation model and the actual 3D entity, equivalent treatment should be carried out. The principle is to ensure the total heat loss of the motor remains unchanged, and the equivalent treatment method of heat dissipation coefficient is as follows:

$$\sum \alpha_1 S_1 = \alpha_2 S_2. \tag{8}$$

In (8), α_1 is the surface heat dissipation coefficient of each part of the solid motor surface; S_1 is the surface area of

each part of the solid motor; α_2 is the equivalent convective heat dissipation coefficient of a two-dimensional model of the motor; S_2 is the outer surface area of the motor stator.

4.3.2. Calculation of End Heat Dissipation Coefficient. The airflow in the end space of a motor is usually more complicated than the flow on its outer surface. The cooling calculation of this area at the end of the motor is the most difficult part of the motor. Equation (9) was obtained by curve fitting the convective heat transfer coefficient of the surface in contact with the end space fluid and the local fluid velocity [22].

$$h_{me} = k_1\left(\frac{P_z}{P_o}\right) * \left[1 + k_2\left(\frac{P_z}{P_o}\right)^{(k_3-0.5)} * v_{e1}^{k_3}\right]. \quad (9)$$

In (9), k_1, k_2, and k_3 are curve fitting coefficients. P_z/P_o is the pressure ratio. v_{el} is the reference speed.

4.3.3. Equivalent Heat Transfer Coefficient of the Air Gap. When the motor moves, the air gap is affected by the tangential motion of the rotor due to rotor rotation. At the same time, the balance block and the blade on the rotor end ring will disturb the airflow, so the heat transfer on the rotor surface will be greatly affected. In this paper, the Nusselt criterion is introduced to determine the heat transfer coefficient of the air gap [23, 24]. The heat exchange capacity λ_{eff} of flowing air in the air gap is described by the thermal conductivity of the stationary fluid.

When $R_e > R_{ecr}$, the motor is in a turbulent state:

$$\lambda_{\text{eff}} = \frac{N_u \lambda_{\text{air}}}{l_\delta}. \quad (10)$$

When $R_e < R_{ecr}$, the motor is in a laminar flow state:

$$\lambda_{\text{eff}} = 0.0019\left(\frac{D_r}{D_s}\right)^{-2.9084} R_{ecr}^{0.461\ \ln(3.33361-\eta)}. \quad (11)$$

In (10) and (11), N_u is the Nusselt coefficient; l_δ is the length of the air gap; D_r is the inner diameter of the rotor; D_s is the inner diameter of the stator; R_e is Reynolds coefficient; R_{ecr} is the critical Reynolds coefficient.

5. Temperature Rise Law of Motor under the Influence of Multiple Factors

5.1. Temperature Rise Calculation at Different Ambient Temperatures during the Full Load Operation. The internal parts of the motor are assumed to have uniform heating. According to the symmetry and heat conduction characteristics of the motor, the whole motor model is established. Because the heat transfer in the motor is symmetrical, the heat of the symmetrical part is consistent, and the symmetrical surface can be treated as an adiabatic surface. The loss characteristics of the motor at full load operation are shown in Figure 2.

The simulation results are imported into Fluent software for finite element simulation of temperature field. When the ambient temperature is −30°C, the temperature of each part of the motor is shown in Figure 3.

It can be seen from Figure 3 that the highest temperature occurs at the rotor end, and the highest temperature is 9°C.

Similarly, when the ambient temperature is 25°C, the temperature of each part of the motor is shown in Figure 4.

It can be seen from Figure 4 that the highest temperature occurs at the rotor end, and the highest temperature is 64°C.

Similarly, when the ambient temperature is 40°C, the temperature of each part of the motor is shown in Figure 5.

It can be seen from Figure 5 that the highest temperature occurs at the rotor end, and the highest temperature is 79.4°C.

The simulation results of the Fluent motor temperature are summarized. Temperature values and temperature appreciation under different ambient temperatures are shown in Figures 6 and 7 when the motor has run at full load.

It can be seen from Figures 6 and 7 that the ambient temperature has almost no influence on the temperature rise of ordinary small and medium-sized motors. If this rule is ignored, it is easy to make a false diagnosis about the motor's health.

5.2. The Temperature Rise of the Motor Varies with the Load Rate and the Ambient Temperature. When the motor runs under different ambient temperatures and different load conditions, the temperature rise state of the motor will also change. In this paper, the influence of ambient temperature and load rate on the temperature and temperature rise of the motor is studied by establishing the curves of the temperature rise of the motor with the load rate at different ambient temperatures.

Considering the complexity of the overall structure of the motor, combined with the experimental test of the motor parts placed by the sensor, the motor model is established. Calculate the temperature values and temperature appreciation of the stator, winding, and rotor of the motor operating at 0–100% load rate at −30°C, 20°C, 25°C, 30°C, and 40°C.

The steady-state temperature and temperature rise of the motor stator under different ambient temperatures and load rates are shown in Figures 8 and 9.

The simulation results show that the amplitude and speed of stator temperature rise are affected by the load rate of the motor. At the same ambient temperature, the temperature rise rate of the motor stator increases with the increase of the load rate. The variation ratio of stator temperature rise to 0–60% load, 60%–80% load, and 80%–100% load is 1 : 4.6 : 6.9.

The steady-state temperature values and temperature rise values of the windings of different loads for the motor at five different ambient temperatures are shown in Figures 10 and 11.

The simulation results show that the amplitude and speed of temperature rise of motor winding are affected by the load rate of the motor. At the same ambient temperature, the temperature rise rate of motor winding increases with the increase of load rate. The temperature rise of motor winding in 0–60% load, 60%–80% load, and 80%–100% load is 1 : 3.3 : 7.4.

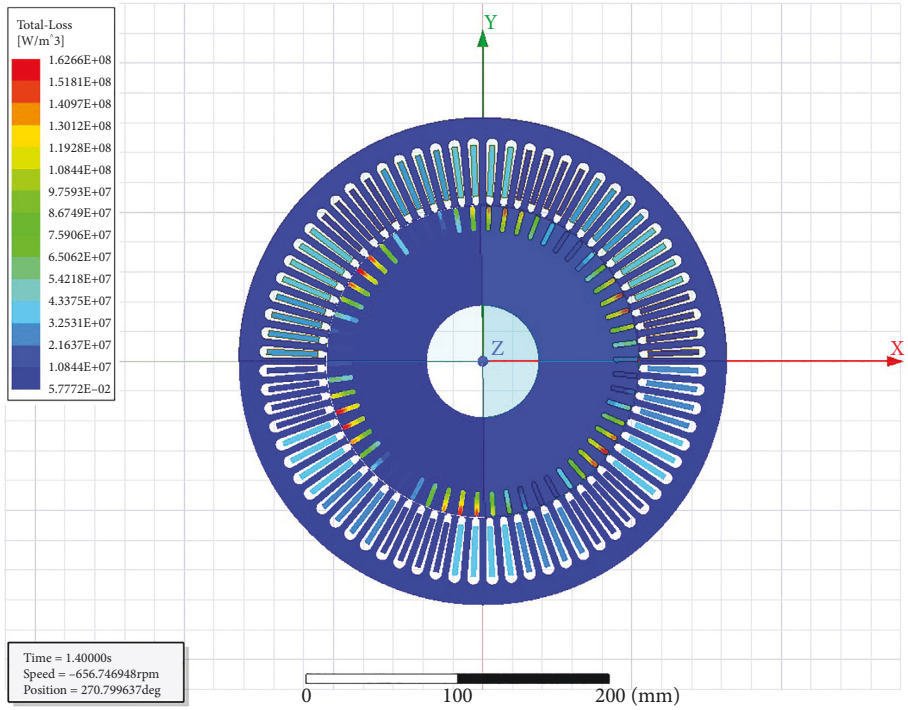

Figure 2: Motor loss characteristics during the full load operation.

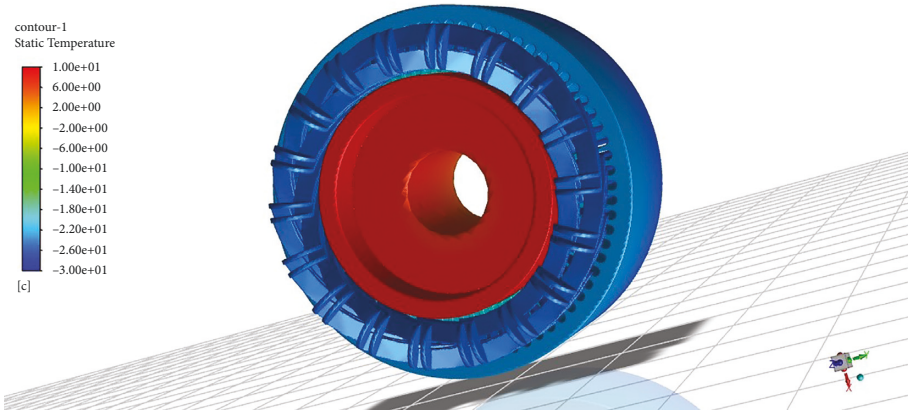

Figure 3: −30°C motor temperature simulation.

The steady-state temperature values and temperature appreciation of the motor rotor with different load rates under five ambient temperatures are shown in Figures 12 and 13.

The simulation results show that the amplitude and speed of rotor temperature rise are affected by the load rate of the motor. At the same ambient temperature, the temperature rise rate of the rotor increases with the increase of the load rate. The variation ratio of rotor temperature rises to 0–60% load, 60%–80% load, and 80%–100% load is 1 : 3.3 : 7.4.

To sum up, the motor temperature rise is affected by the motor load rate. At the same ambient temperature, the temperature rise rate of the motor increases with the increase of the load rate, showing a three-stage change. Under 0–60% load, 60%–80% load, and 80%–100% load, the temperature rise rate of the motor is slow, fast, and fastest. When the motor runs under different loads, the greater the load, the greater the excitation current, the longer the start time, and the greater the temperature rise change rate during the start process. In the process of motor health diagnosis, if the influence of motor load rate on motor temperature and temperature rise is not considered, the monitoring system will make a wrong diagnosis of motor health status.

To further study the temperature rise distribution law among the rotor, winding, and stator of the motor, the temperature rise curves of the rotor, winding, and stator

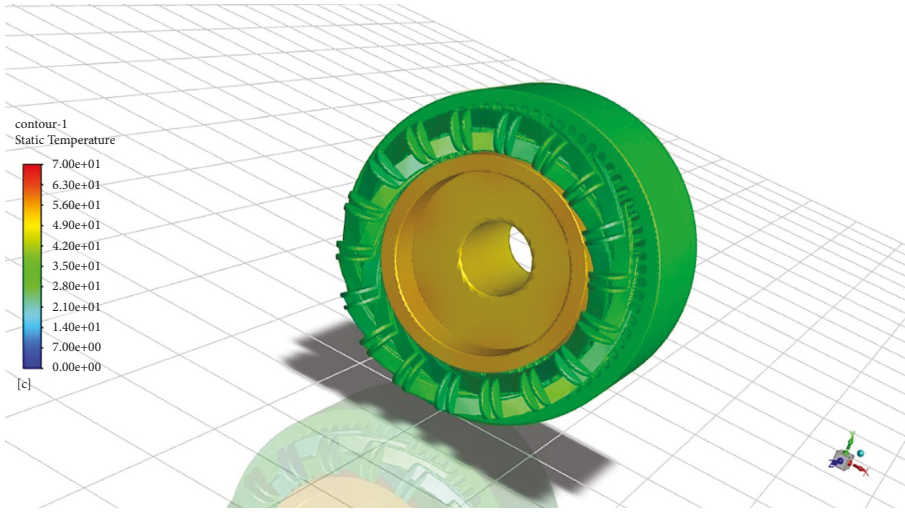

Figure 4: 25°C motor temperature simulation.

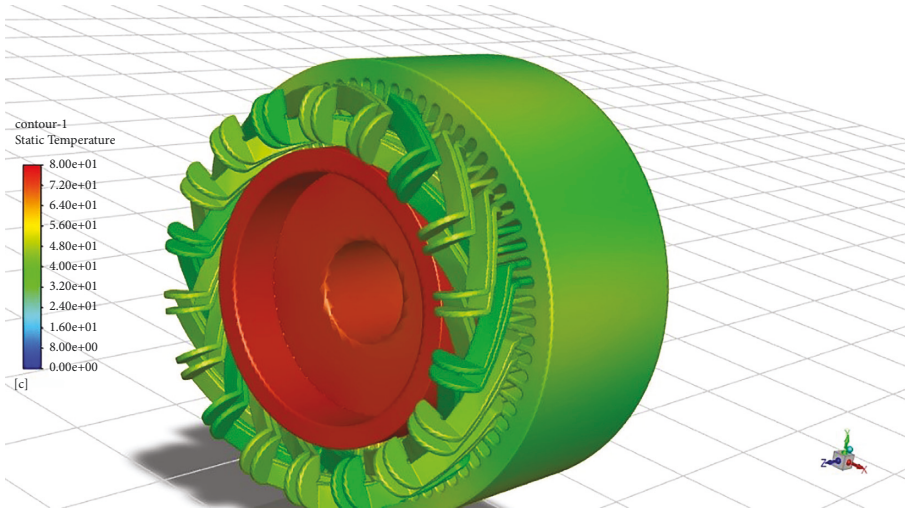

Figure 5: 40°C motor temperature simulation.

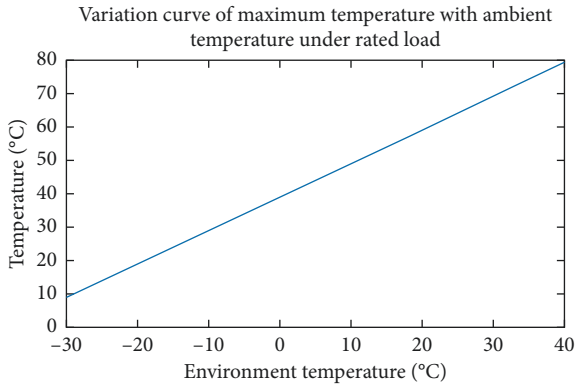

Figure 6: Variation curve of maximum temperature with ambient temperature under rated load.

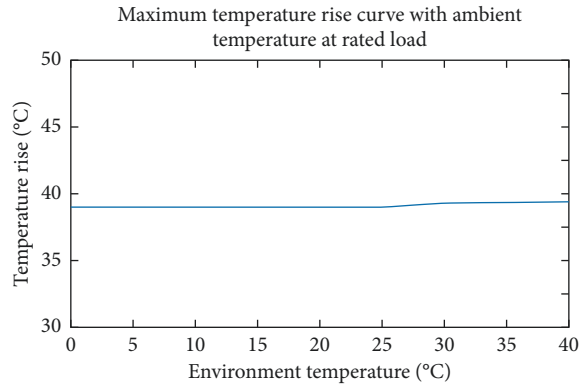

Figure 7: Maximum temperature rise curve with ambient temperature at rated load.

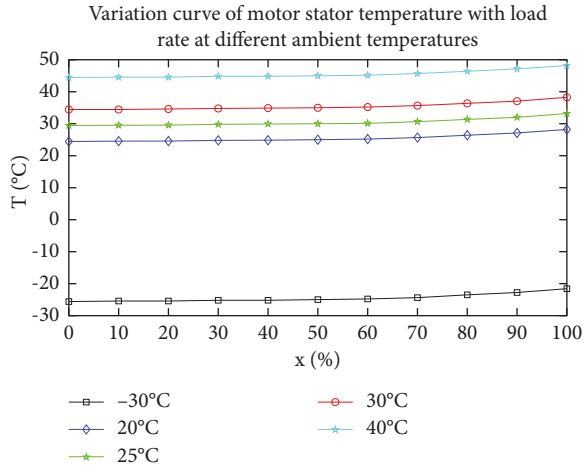

Figure 8: Variation curve of motor stator temperature with load rate at different ambient temperatures.

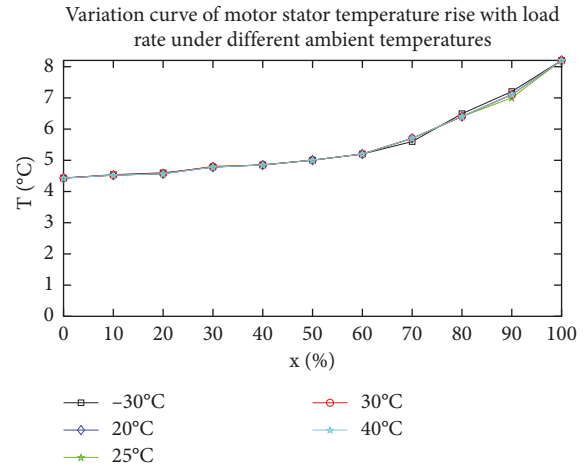

Figure 9: Variation curve of motor stator temperature rise with load rate under different ambient temperatures.

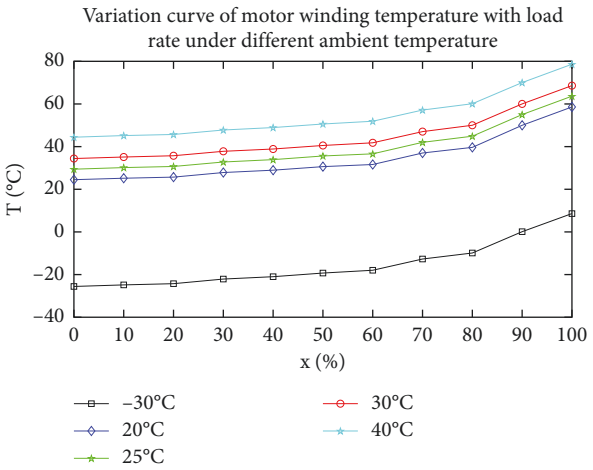

Figure 10: Variation curve of motor winding temperature with load rate under different ambient temperature.

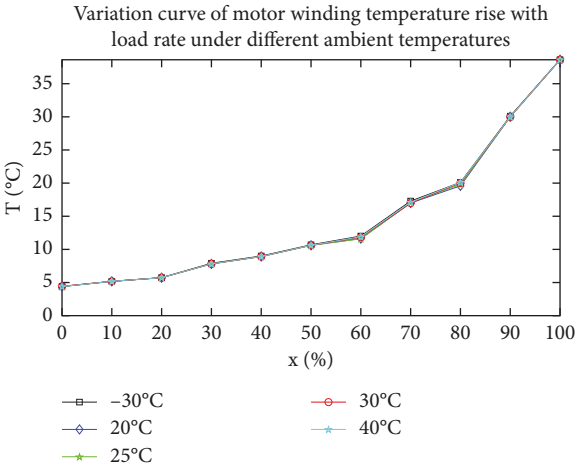

Figure 11: Variation curve of motor winding temperature rise with load rate under different ambient temperatures.

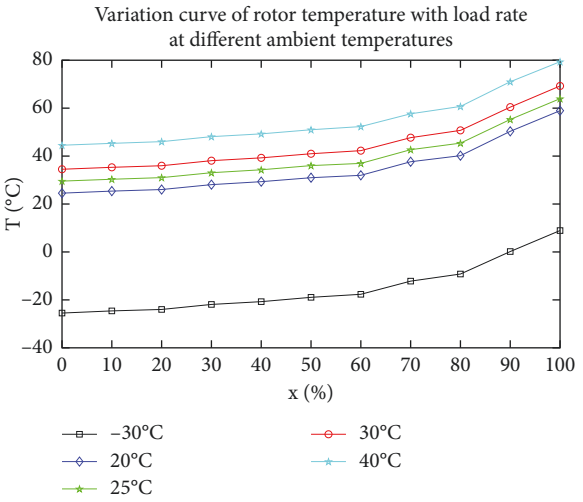

Figure 12: Variation curve of rotor temperature with load rate at different ambient temperatures.

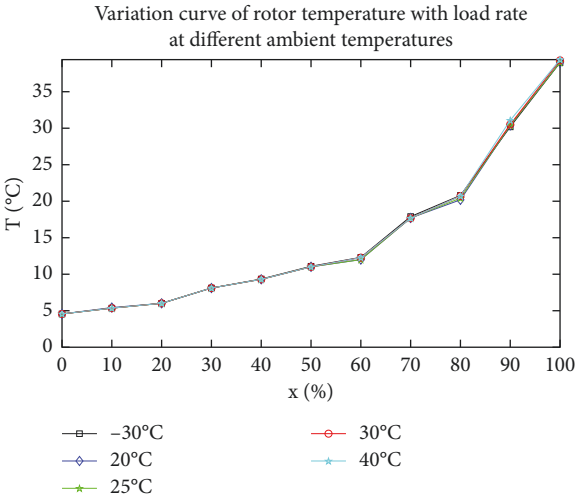

Figure 13: Variation curve of rotor temperature with load rate at different ambient temperatures.

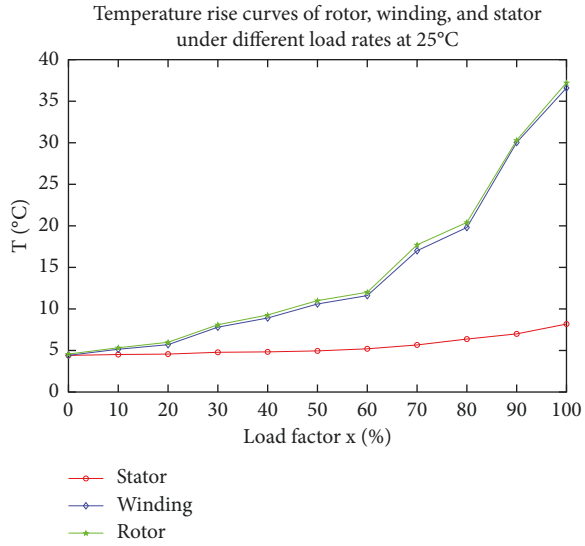

Figure 14: Temperature rise curves of rotor, winding, and stator under different load rates at 25°C.

Table 4: Maximum temperatures of rotor, winding, and stator under different load rates at 25°C.

Load factor	Stator temperature	Winding temperature	Rotor temperature
0	29.43	29.4	29.54
10%	29.52	30.16	30.34
20%	29.57	30.7	31
30%	29.8	32.8	33.1
40%	29.85	33.9	34.3
50%	30	35.6	36
60%	30.2	36.6	37
70%	30.7	42	42.7
80%	31.4	44.8	45.4
90%	32	55	55.3
100%	33.2	61.6	62

under different load rates of the motor at 25°C are drawn as shown in Figure 14.

Figure 14 shows the distribution rule of temperature rise difference between rotor, winding, and stator at standard temperature. Because some motors are manufactured without temperature sensors, especially the rotor cannot be equipped with temperature sensors. Therefore, the rotor temperature value and temperature appreciation cannot be obtained. According to the law of this paper, the stator temperature value and temperature rise can be used to check the motor winding and rotor temperature value and temperature rise, improve the accuracy of motor health diagnosis, and reduce the number of temperature detectors in the monitoring system, saving investment.

The specific values of temperature and temperature rise in the temperature rise curves of the rotor, winding, and stator under different load rates in Figure 14 at 25°C are refined into Table 4 and 5.

By combining the temperature rise curves of the rotor, winding, and stator at different load rates in Figure 14 with the temperature rise threshold of the motor at 25°C, the

Table 5: Maximum temperature rise of rotor, winding, and stator under different load rates at 25°C.

Load factor	Stator temperature rise	Winding temperature rise	Rotor temperature rise
0	4.43	4.4	4.54
10%	4.52	5.16	5.34
20%	4.57	5.7	6
30%	4.8	7.8	8.1
40%	4.85	8.9	9.3
50%	5	10.6	11
60%	5.2	11.6	12
70%	5.7	17	17.7
80%	6.4	19.8	20.4
90%	7	30	30.3
100%	8.2	36.6	37

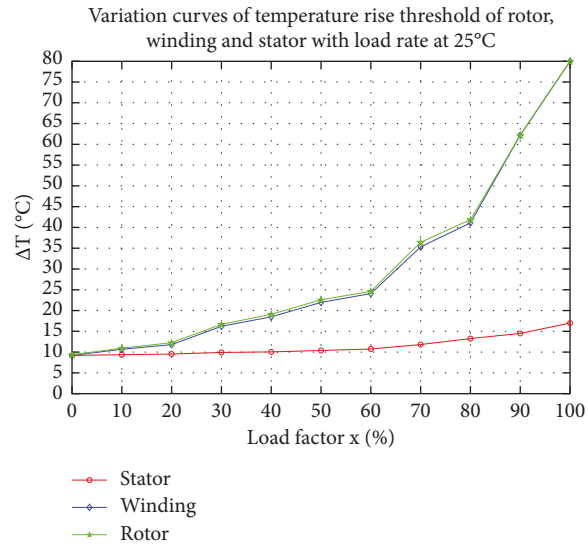

Figure 15: Variation curves of temperature rise threshold of rotor, winding, and stator with load rate at 25°C.

temperature rise threshold of the rotor, winding, and stator with the load rate is obtained as shown in Figure 15.

According to the curve of temperature rise threshold of rotor, winding, and stator with load rate at 25°C and the conversion rule of temperature and temperature rise among stator, winding, and rotor at different load rates, a dynamic threshold judgment system that can accurately warn the motor overheating problem at any load rate is established. The system can more accurately judge whether the temperature rise of the motor exceeds the temperature rise threshold under different load rates, and more accurately judge the motor's health condition under light load. It provides an important theoretical basis for the design of motor temperature and temperature rise prediction system, and also provides a method support for the thermal health diagnosis and early warning of intelligent motor system.

6. Conclusion

This paper takes an 11 kW three-phase asynchronous motor as an example, using ANSYS software to establish the motor

temperature rise model based on the finite element method. The thermal conductivity coefficient and surface heat dissipation coefficient of each part of the motor are determined. According to the electromagnetic field calculation, the distribution of iron loss, copper loss, and mechanical loss of the motor is obtained. Based on the finite element method, the temperature field of the motor is simulated, and the electromagnetic and thermal parameters of the motor are systematically analyzed and calculated. The loss distribution and temperature rise distribution of motor under different ambient temperature and load conditions are obtained. This paper draws the following conclusions:

(1) The variation of motor temperature rise with ambient temperature and load rate is analyzed in detail. The temperature rise distribution and the dynamic curve of temperature rise threshold are presented considering the influence of ambient temperature and load rate.

(2) At the same ambient temperature, the temperature rise rate of the motor increases with the increase of the load rate, showing a three-stage change. Under 0–60% load, 60%–80% load, and 80%–100% load, the temperature rise rate of the motor is slow, fast, and fastest. The proportion of stator temperature rise is 1 : 4.6 : 6.9, the proportion of winding temperature rise is 1 : 3.3 : 7.4, and the proportion of rotor temperature rise is 1 : 3.2 : 7.2. It is proved that there is no linear relation between the temperature rise rate and the load rate. This rule needs to be taken into account in motor health diagnosis.

(3) At the same load rate, the temperature rise of the motor has nothing to do with the ambient temperature. So pay special attention to the drastic changes in temperature rise when the ambient temperature changes. Prevent the wrong diagnosis of the health of the motor.

(4) The law of temperature rise difference between rotor, winding, and stator is obtained. According to the relevant laws, the temperature rise of the stator can be used to check the temperature rise of motor winding and rotor, improve the accuracy of motor health diagnosis, reduce the number of temperature detectors in the monitoring system, and save investment.

The variation law of motor temperature rise influenced by multiple factors makes up for the defect that the traditional temperature measurement method does not consider the influence of load factors, provides an important theoretical basis for the design of the same type of motor and operation monitoring system, and contributes to verifying the rationality of the design of motor monitoring system.

Data Availability

The data used to support the findings of this study are available from the corresponding author upon request.

Conflicts of Interest

The authors declare that they have no conflicts of interest.

References

[1] V. Madonna, P. Giangrande, L. Lusuardi, A. Cavallini, C. Gerada, and M. Galea, "Thermal overload and insulation aging of short duty cycle, aerospace motors," *IEEE Transactions on Industrial Electronics*, vol. 67, no. 4, pp. 2618–2629, 2020.

[2] M. Gulec, M. Aydin, J. Nerg, P. Lindh, and J. J. Pyrhonen, "Magneto-thermal analysis of an axial-flux permanent-magnet-assisted eddy-current brake at high-temperature working conditions," *IEEE Transactions on Industrial Electronics*, vol. 68, no. 6, pp. 5112–5121, 2021.

[3] P. T. Luu, J. Lee, and J. W. Park, "Electromagnetic and thermal analysis of permanent-magnet synchronous motors for cooperative robot applications," *IEEE Transactions on Magnetics*, vol. 56, no. 3, pp. 1–4, 2020.

[4] T. Li, Y. Zhang, Y. Liang, A. I. Qiang, and H. Dou, "Thermal analysis and research of axial flux hub motor," *Journal of Engineering and Thermophysics*, vol. 42, pp. 1561–1568, 201.

[5] Y. Wu, H. Song, X. Dong, H. Wu, and F. Xin, "Equivalent thermal key parameters of multi-field coupling motor temperature field," *Engineering Journal of Wuhan University (Engineering Edition)*, vol. 54, pp. 438–444, 201.

[6] Y. Ma, J. Li, and J. Liu, "Thermal analysis and research of permanent magnet brushless motor based on hybrid electric vehicle," *Journal of Engineering and Thermophysics*, vol. 39, no. 11, pp. 2525–2531, 2018.

[7] Y. Liu, Z. Yu, and X. Zhang, "Heat flow field simulation and parameter sensitivity analysis of large-capacity high-speed permanent magnet motor," *Electric Machines and Control Applications*, vol. 45, pp. 103–107, 2018.

[8] Y. Gao, J. Cao, C. Zou, and Q. Wang, *Electric machines and control applications*, vol. 46, 2019.

[9] B. Ge, X. Xu, D. Tao, J. Han, and L. Wang, "Gas friction loss in stator ventilation ducts of the drive motor for the cooling medium in a high-temperature gas-cooled reactor," *IEEE Transactions on Industrial Electronics*, vol. 66, no. 1, pp. 114–123, 2019.

[10] J. Zhang, Z. Zhang, Y. Xia, and L. Yu, "Thermal analysis and management for doubly salient brushless DC generator with flat wire winding," *IEEE Transactions on Energy Conversion*, vol. 35, no. 2, pp. 1110–1119, 2020.

[11] J. Zhang, Z. Zhang, and L. Yu, "Thermal deformation analysis of water cooling doubly salient brushless DC generator with stator field winding," *IEEE Transactions on Industrial Electronics*, vol. 67, no. 4, pp. 2700–2710, 2020.

[12] Y. Zhang, X. Wang, T. Han, and R. Wang, "Electric vehicle motor aging model test based on winding temperature rise," *Journal of Automotive Engineering*, vol. 8, pp. 50–53, 2018.

[13] Y. Wu, Z. Zhang, and P. Jiaqi, "Design and temperature field analysis of new water-cooling structure for axial flux permanent magnet motor with high power density," *Proceedings of the CSEE*, vol. 41, no. 24, pp. 8295–8305, 201.

[14] Y. Jiang, T. Huang, X. Zhou, Y. Ning, Y. Zhang, and C. Qi, "Design method for reducing temperature rise of high speed permanent magnet motor in vacuum environment," *Small and Special Electrical Machines*, vol. 50, 202.

[15] GB/T 11021-1989, *Evaluation and Classification of Heat Resistance of Electrical Insulation*, 1989.

[16] GB/T 11021-2014, *Heat Resistance and Expression Method of Electrical Insulation*, 2014.

[17] K. Atallah, Z. Q. Zhu, and D. Howe, "An improved method for predicting iron losses in brushless permanent magnet DC

drives," *IEEE Transactions on Magnetics*, vol. 28, no. 5, pp. 2997–2999, 1992.

[18] M. A. Mueller, S. Williamson, T. J. Flack et al., "Calculation of iron losses from time-stepped finite-element models of cage induction machines," in *Proceedings of the IEEE International Electric Machines and Drives Conference*, vol. 9, p. 88, Anterbury, UK, 1995.

[19] C. I. McClay and S. Williamson, "The variation of cage motor losses with skew," *IEEE Transactions on Industry Applications*, vol. 36, no. 6, pp. 1563–1570, 2000.

[20] W. Tong, S. Wu, and R. Tang, "Totally enclosed self-circulation axial ventilation system design and thermal analysis of a 1.65-MW direct-drive PMSM," *IEEE Transactions on Industrial Electronics*, vol. 65, no. 12, pp. 9388–9398, 2018.

[21] G. Du, W. Xu, J. Zhu, and N. Huang, "Power loss and thermal analysis for high-power high-speed permanent magnet machines," *IEEE Transactions on Industrial Electronics*, vol. 67, no. 4, pp. 2722–2733, 2020.

[22] L. Diao and X. Guo, "Analysis of temperature field characteristics of high-voltage and high-power cage induction motors under different loads," *Explosion-Proof Motors*, vol. 55, no. 05, pp. 16–20, 2020.

[23] L. Li, J. Zhang, H. Yan, and J. Yu, "Calculation of three-dimensional temperature field and heat conduction optimization of high power density motor," *Proceedings of the Chinese Society for Electrical Engineering*, vol. 36, no. 13, 2016.

[24] X. Huang, Q. Tan, L. Li, J. Li, and Z. Qian, "Winding temperature field model considering void ratio and temperature rise of a permanent-magnet synchronous motor with high current density," *IEEE Transactions on Industrial Electronics*, vol. 64, no. 3, pp. 2168–2177, 2017.